*fluids*

MDPI

*Article*

# Experimental Investigations of Capillary Flow in Three-Dimensional-Printed Microchannels

**Behrouz Pirouz [1,*], Seyed Navid Naghib [1], Diamante Chirillo [2], Hana Javadi Nejad [1] and Patrizia Piro [1]**

[1] Department of Civil Engineering, University of Calabria, 87036 Rende, Italy; navid.naghib@unical.it (S.N.N.); hana.javadi@unical.it (H.J.N.); patrizia.piro@unical.it (P.P.)
[2] Faculty of Medicine and Surgery, Università di Roma Tor Vergata, 00133 Rome, Italy; diamantechirillo97@gmail.com
* Correspondence: behrouz.pirouz@unical.it

**Abstract:** In recent years, the application of microfluidic devices has increased, and three-dimensional (3D) printers for fabricating microdevices could be considered a suitable technique but, in some cases, may confront some issues. The main issues include channel roughness values, print orientation due to the 3D printer's setup, filament materials, nozzle specifications, and condition. This study aims to analyze the capillary-driven flow in microdevices produced by 3D printers. Therefore, four 3D printer-based microchannels were investigated, and the capillary-driven flow of five liquids with different viscosities and contact angles was evaluated experimentally. The experimental results were compared with theoretical calculations using the Lucas−Washburn equation, and the impact of the width, length, and closed and open microchannel on flow behaviors was explored. The experimental results showed that the peak velocity for open and closed microchannels decreases with the length. Moreover, there were differences in flow behavior between open and closed microchannels. For the former, the maximum average velocity appeared in the microchannel with a width of 400 μm, while for the latter, it was for a width of 1000 μm. In addition, the flow velocity decreased when the viscosity increased, regardless of microchannel width. The decrease was more pronounced for the lower-viscosity liquids (ethanol and water) and smaller for the higher-viscosity ones (coffee and olive oil). Finally, the advantages and challenges of 3D printer-based microdevices are presented.

**Keywords:** microfluid; viscosity; capillary flow; microchannel; 3D printer

check for updates

Academic Editor: Moran Wang

Received: 12 February 2025
Revised: 27 March 2025
Accepted: 1 April 2025
Published: 2 April 2025

**Citation:** Pirouz, B.; Naghib, S.N.; Chirillo, D.; Javadi Nejad, H.; Piro, P. Experimental Investigations of Capillary Flow in Three-Dimensional-Printed Microchannels. *Fluids* **2025**, *10*, 91. https://doi.org/10.3390/fluids10040091

**Copyright:** © 2025 by the authors. Licensee MDPI, Basel, Switzerland. This article is an open access article distributed under the terms and conditions of the Creative Commons Attribution (CC BY) license (https://creativecommons.org/licenses/by/4.0/).

## 1. Introduction

Microfluidics, a cutting-edge field at the intersection of engineering and biology, has gained significant attention for its applications in precise fluid control. Microfluidics represents a significant feature in numerous micro-manufactured devices, typically associated with the micron scale (1 μm–1000 μm). However, the definition does not solely depend on the geometric size of the channel, but also on governing physical principles [1], and there is no strict boundary for the definition of microfluidics. In some studies, a channel with a width of 3000 μm is considered to be a microfluidic channel [2], and devices with channel diameters of 2000 μm are categorized as microfluidic devices [3]. In fact, for widths less than 10 mm (10,000 μm), the fluid bulk properties (like viscous drag and inertial forces) and interfacial properties (like interfacial tension and capillary force) are dominant [4].

Microscopic capillary structures are crucial components within numerous microfluidic devices [5], facilitating swift operations such as mixing [6–8], separation [9], and diagnostics with minimal sample fluid volumes [10]. Additionally, microchannels play a vital role in

micro-molding [7], capillary flow in pavements [11,12], printers, and 3D printing [13,14]. Capillary action, also known as capillary flow, plays a crucial role in numerous scientific and manufacturing processes, such as extensive use in medical devices, facilitating precise fluid control in applications like diagnostic tools [15], drug delivery systems [16], nanotechnology, biomedicine [17], and more.

Capillary-driven flow is the ability of a fluid to flow in narrow channels without external forces, which depends not only on the liquid properties but also on the channel surface condition and material [18]. Therefore, it combines cohesive and adhesive forces between the liquid and the microchannel surface and the liquid molecules. The main parameters in this subject include wettability, surface tension, and contact angle [19]. Wettability is a key factor in how a liquid interacts with a solid surface, exhibiting the flow velocity within the microchannels [20]. A surface is deemed wettable when the contact angle of a liquid on that surface is less than 90°. Microchannels featuring wettable surfaces create a concave liquid–air interface, resulting in negative capillary pressure that spontaneously draws liquid into the conduit through capillary action. Conversely, the interface becomes convex for angles greater than 90°, leading to positive capillary pressure that ejects liquid out of the channel [21]. Surface tension is another critical parameter that is a driving force in determining the shape and stability of the meniscus formed within the microchannels [22]. The interactions between the liquid and microchannel surfaces, influenced by surface tension, could show distinct behaviors, revealing the underlying physics of the governing capillary flow. Additionally, the contact angle, representing the angle at which the liquid meets the solid surface [23], has emerged as a key determinant in dictating the capillary flow and the overall wetting behavior.

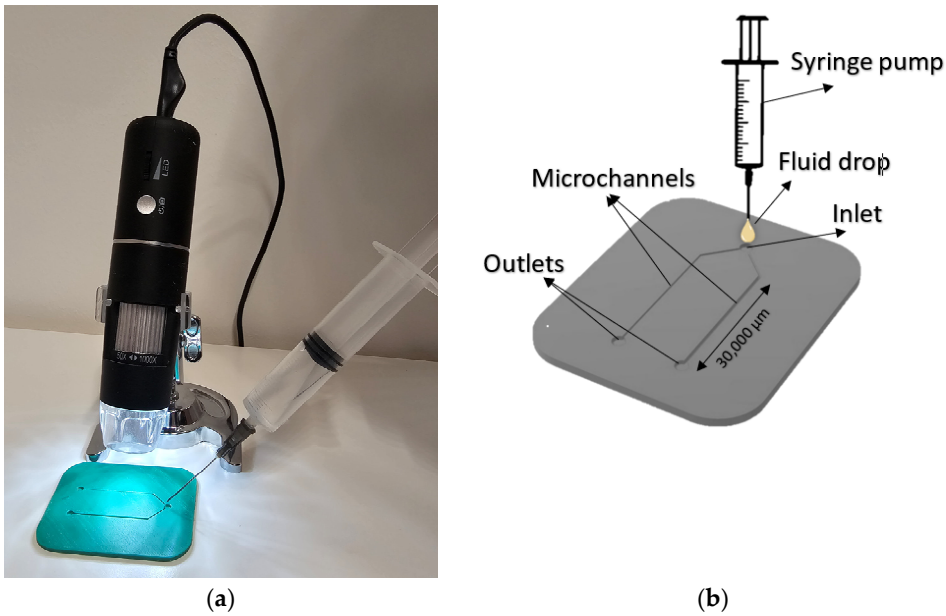
Keshmiri et al. [24] investigated the capillary filling dynamics of different fluids in different microchannels. They compared experimental results with the theoretical Lucas–Washburn equations [25] and concluded that their experimental results were in good agreement with the theoretical results in both microchannels treated with Hexamethyldisilazane (HMDS) and untreated microchannels. Moreover, their analysis demonstrated the importance of using dynamic contact angles instead of static contact angles in the calculations of the microchannel capillary flows. Yang et al. [26] studied capillary-driven flow in hydrophobic surfaces in rectangular and curved cross-sections of open microchannels with different widths. They compared their experimental data with the theoretical equation and showed the linear dependency of the square of the meniscus position on the flow time ($x^2 \sim t$) in both rectangular and curved cross-section open microchannels. Moreover, their study showed that the capillary flow velocity decreases with the increase in microchannel widths. Bao and Nagayama [27] investigated the optimization of capillary flow in open rectangular hydrophilic Si-fabricated microchannels ranging from 18 μm to 375 μm in width. They concluded that the optimal capillary flow velocity value was achieved at the aspect ratio (width to height) of the two. Moreover, their results demonstrated that the imbibition rate increases with the rise in the hydraulic diameter. Lade et al. [28] examined capillary flow dynamics in 3D-printed manufactured microchannels. They compared the devices based on four different 3D printing techniques, including fused deposition modeling (FDM), stereolithography (SLA), MultiJet modeling (MJM), and selective laser sintering (SLS), over different time scales, including short, intermediate, and long. The analyses revealed that the high surface roughness of 3D printers could cause start-stop motion in the microchannel. Moreover, the cross-sectional shapes on the microchannel surfaces could affect the expected capillary flow velocity. Truesdell and Saunders [29] analyzed oscillatory flow on the developed microfluidic device with a 3D printer, and their results showed the simplicity and reliability of the 3D printer for LOC devices.

In recent years, extensive research has been conducted to understand the behavior of capillary-driven flow in microfluidic devices and microchannels. A literature review shows that the studies on different fluid behaviors in 3D printer-based microfluidic conditions are sparse. Therefore, this study aims to analyze the capillary-driven flow of different fluids in microdevices fabricated by a 3D printer. In this regard, this paper investigates four sizes of closed and open microchannels with widths of 400, 800, 1000, and 2000 µm, and the capillary-driven flow of five liquids with different flow properties, such as viscosity and contact angles, is evaluated. The impact of width and length are evaluated theoretically using the Lucas−Washburn equation and experimentally. Based on the results, the advantages and challenges of using 3D-printed microdevices and techniques to decrease the issues are presented. The research results could provide specific scientific insights for applying 3D-printed microfluid devices, paving the way for optimization in microfluidic applications and beyond.

## 2. Materials and Methods

### *2.1. Experimental Setup*

The experimental data were collected at room temperature (20 °C) using an HD digital microscope with a zoom of up to 1000×, as shown in Figure 1. The video capture quality was 100 frames per second (FPS), which can be used for microscale analysis, while a more powerful camera with higher FPS would be required for the nanoscale. The microchannels were filled individually with each selected fluid, and their behavior was observed concerning capillary-driven flow, surface interaction, and overall flow dynamics, as shown in Figure 1a,b. For each test, the board surface was cleaned using ethanol and dried before testing a new liquid.




(**a**) (**b**)

**Figure 1.** The microdevice board: (**a**) capturing method; (**b**) test elements on the board.

The viscosity of distilled water and ethanol was provided by the manufacturers, while for milk, espresso coffee, and olive oil, the measurement of viscosity was performed using Zahn cups [30] No. 1 and No. 2 (ASTM D4212), as shown in Figure 2.

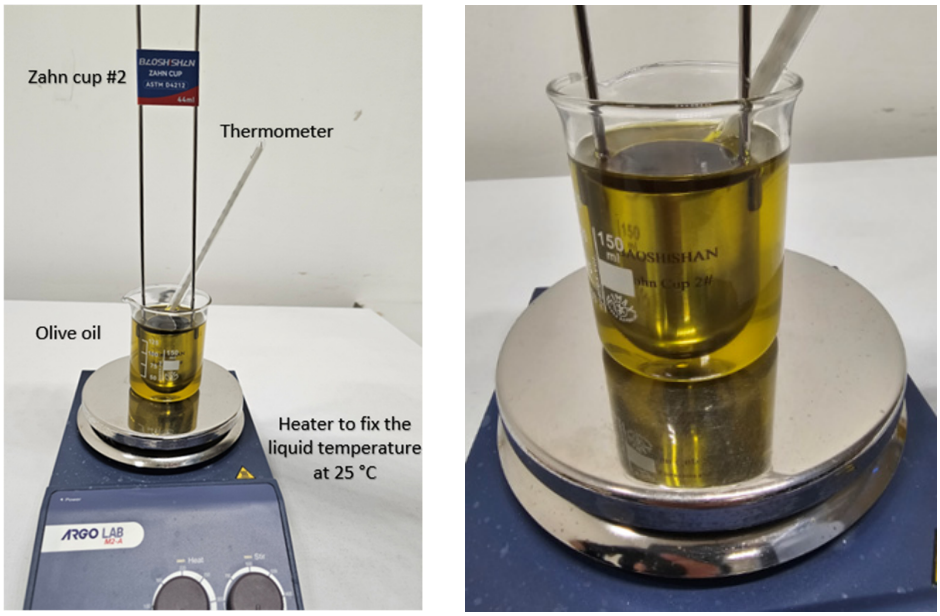



**Figure 2.** Measurements of viscosity with Zahn cups No. 1 and No. 2: (**a**) measurement method; (**b**) testing olive oil viscosity.

### *2.2. 3D Model Development*

The two microdevices were designed using Computer-Aided Design (CAD) software, as shown in Figure 3a, and printed using a 3D printer with a Polylactic Acid (PLA) filament, as shown in Figure 3c,d. The parameters used for the 3D printer include a bed temperature of 45 °C, a nozzle temperature of 210 °C, a layer thickness of 200 µm, and a printing orientation equal to 45°. For the examination of closed microchannels, Polydimethylsiloxane (PDMS) was bonded to the top of the PLA surfaces to avoid leakage from the microchannels, as shown in Figure 3b. As shown in the figures, to compare the impact of microchannel width on the flow speed, two boards with four microchannel widths were produced, including 400 µm, 800 µm, 1000 µm, and 2000 µm, all with the same depth of 1000 µm. Moreover, to ensure the same starting point, the inlet of each of the two microchannels was the same, and the two microchannels on each board were connected to the inlet by a channel with an average width of both.

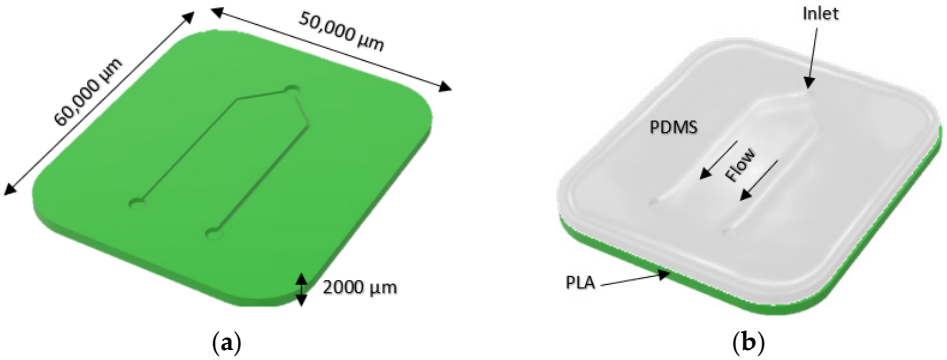
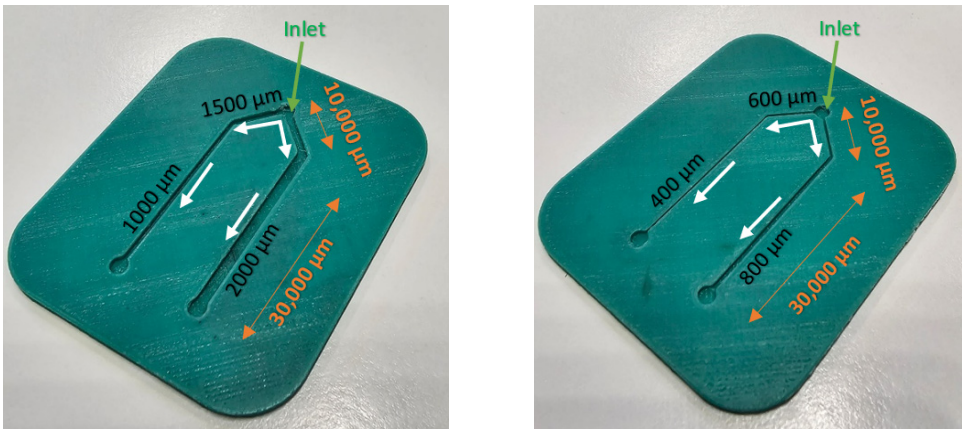



**Figure 3.** *Cont.*




(**c**) (**d**)

**Figure 3.** The two fabricated microdevices: (**a**) Board design; (**b**) PDMS on the board; (**c**) First board with two channels of 1000 µm and 2000 µm; (**d**) Second board with two channels of 400 µm and 800 µm. (Printer model: da Vinci Super XYZ 3D Printers).

### *2.3. Selected Materials' Properties*

The selected Newtonian fluids in this study are reported in Table 1. Water and methanol represent low-viscosity liquids, while milk and coffee are liquids with medium viscosity, with additional complexities due to their colloidal nature. Finally, olive oil represents a high-viscosity fluid.

**Table 1.** The selected materials' properties.

| Material | Viscosity (mPa.s) | Surface Tension [mNm$^{-1}$] | Density [g/mL] | Refs. |
|---|---|---|---|---|
| Distilled water | 1 | 72 | 1 | [31,32] |
| Ethanol | 1.3 | 22.5 | 0.8 | [33,34] |
| Milk | 2 | 46.4 | 1.1 | [35] |
| Espresso coffee | 6 | 46–50 | 1 | [36,37] |
| Olive oil | 78 | 32 | 0.92 | [38] |

### *2.4. Theoretical Analysis*

There are many methods for predicting the flow behaviors in microchannels, such as computational fluid dynamics or simplified equations [39].

One of the widespread equations for the calculation of capillary flow is the Lucas–Washburn (LW) Equation (1) [25,40,41], which is applicable for a uniform cross-section.

$$x(t) = \sqrt{\frac{r\sigma\cos\theta}{2\mu}t} = \sqrt{\frac{D_h\sigma\cos\theta}{4\mu}t} \quad (1)$$

In this equation, the capillary length at time t correlated to the radius r, surface tension σ, viscosity μ, contact angle θ, and time t.

By considering hydraulic diameter instead of r ($D_h$ = 2r) and differentiating Equation (1) with respect to time, Equation (2) can be derived, which is applicable for capillary speed [27].

$$\frac{dx}{dt} = \sqrt{\frac{D_h\sigma\cos\theta}{16\mu t}} \quad (2)$$

The combination of Equations (1) and (2) can result in a time-independent formula, namely Equation (4):

$$\frac{dx}{dt} = \frac{D_h \sigma \cos\theta}{8\mu x} \quad (3)$$

The hydraulic diameter ($D_h$) for the rectangular section can be calculated based on the width (w) and height (H) of the channels, as follows:

$$D_h = \frac{2W.H}{W + H} \quad (4)$$

While the Lucas–Washburn (LW) equation can be used for microchannels, it usually predicts a higher speed for the capillary flow than the experimental test, mainly due to some simplifications such as static contact angle [42].

## 3. Results and Discussion

### *3.1. Flow Velocity of Various Liquids Along Four Sizes of Open Microchannels*

The average velocity along the length of the open microchannels for four widths and five liquids is presented in Figure 4, exhibiting the maximum average velocity for ethanol and the minimum for olive oil. In four of the selected fluids, including water, milk, coffee, and olive oil, it is evident that the flow velocity decreases with the increase in the viscosity, except for ethanol, which showed the opposite behavior, and the flow speed is greater than that of water, despite the lower viscosity of ethanol. The reason could be the lower value of the contact angle in ethanol, which is evaluated in the next section. In addition, the maximum speed for all microchannels occurred at a width of 400 µm, and the minimum at 2000 µm, which is consistent with the study by [26], which concluded that in open microchannels, the flow velocity decreases with the increase in the microchannel's widths.

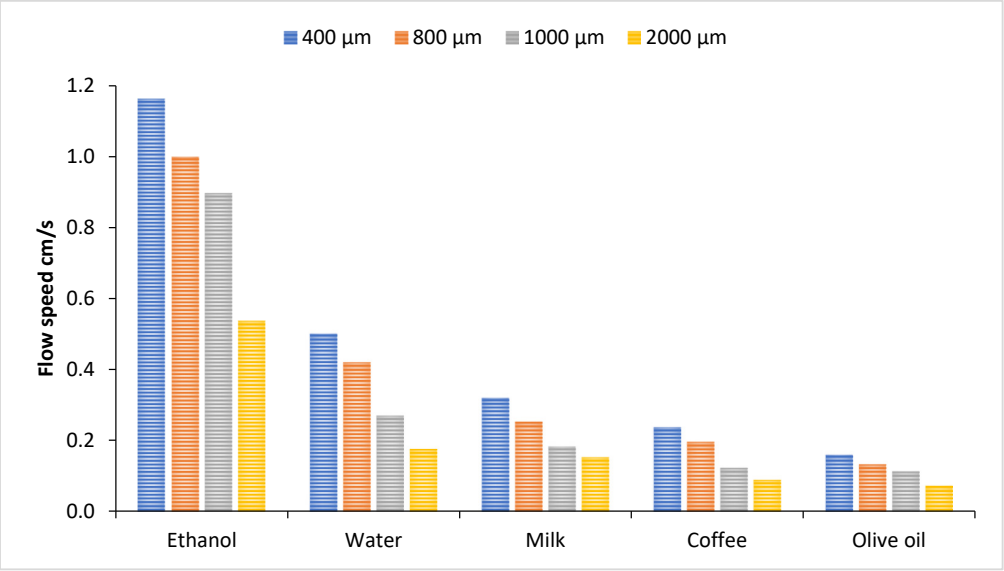



**Figure 4.** The average flow velocity along the length of the open microchannels.

The comparisons of the capillary flow velocities for the five selected fluids across four widths of open microchannels are shown in Figure 5, and the progress of the liquids over time is presented in Figure 6. As can be seen, the flow velocity decreased along the length, and the maximum speeds occurred at the beginning of the microchannel, in agreement with similar studies such as those by Kesmiri et al. [24,27].

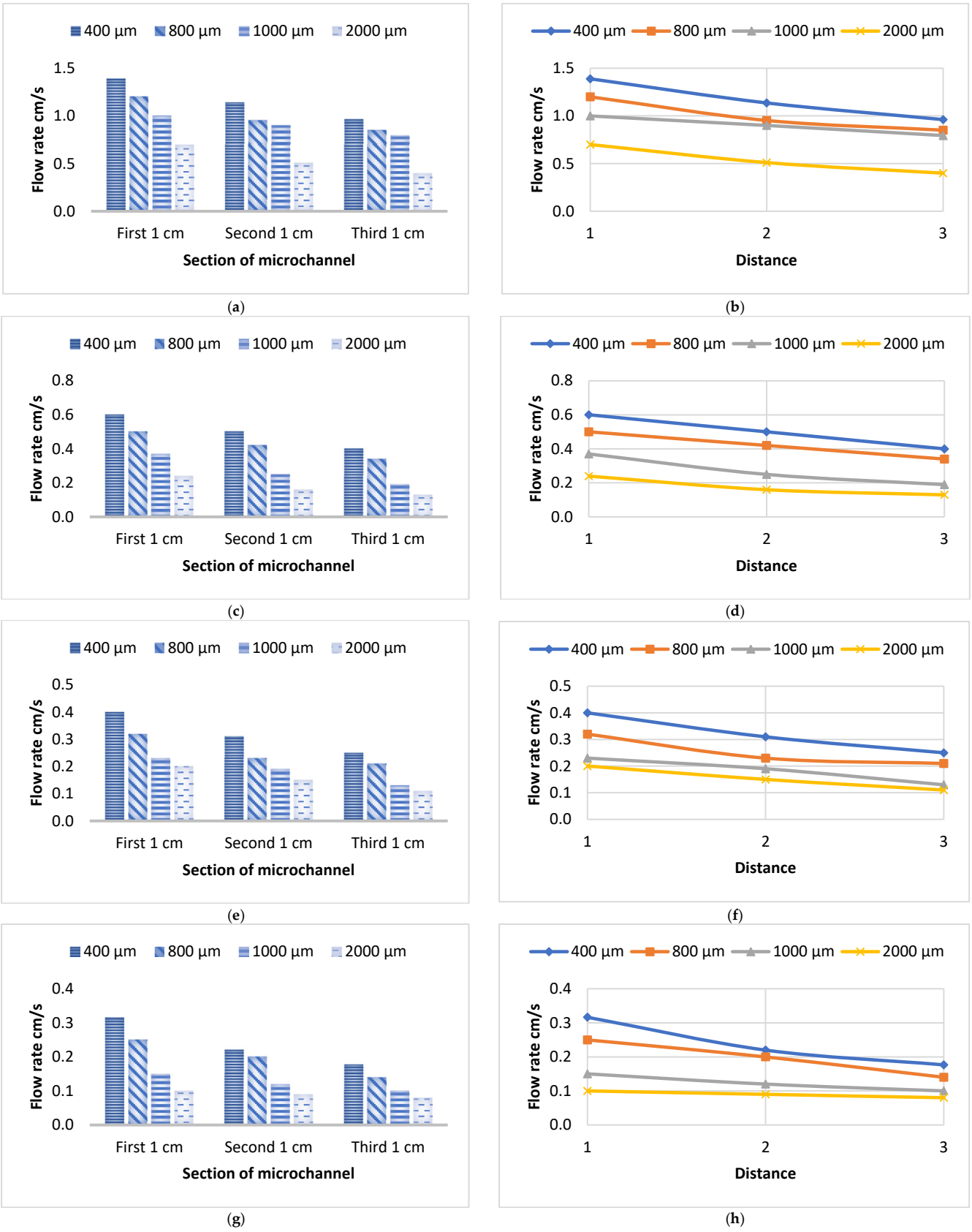
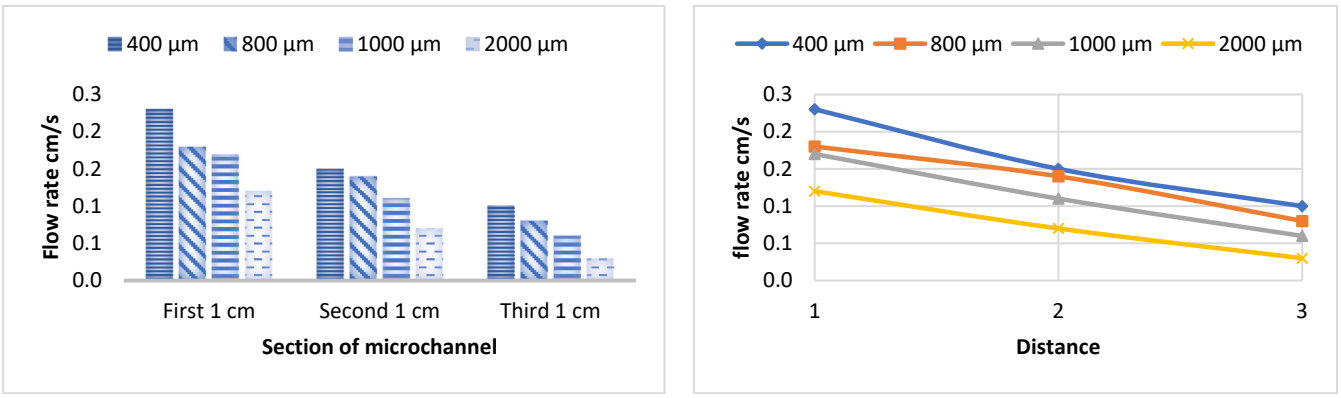
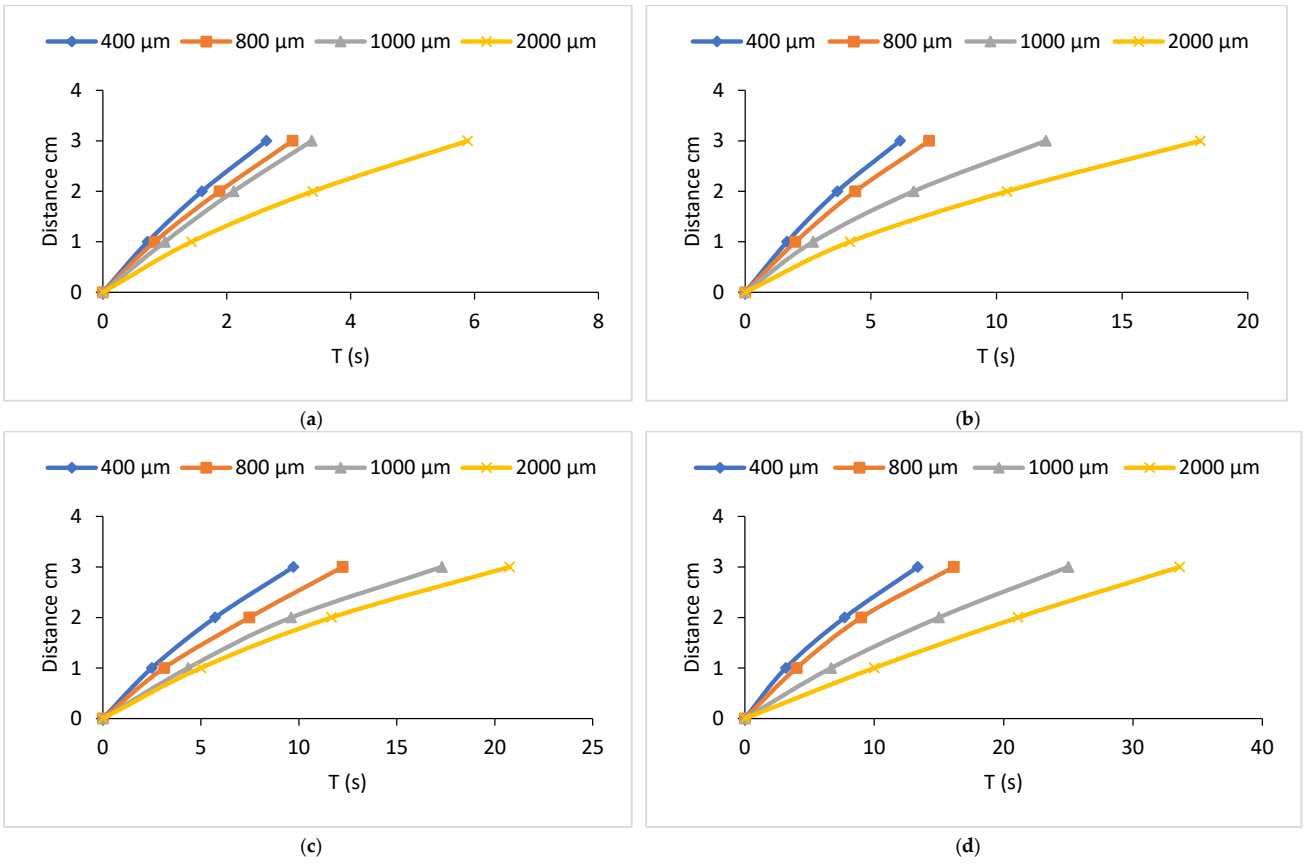



**Figure 5.** *Cont.*




(**i**) (**j**)

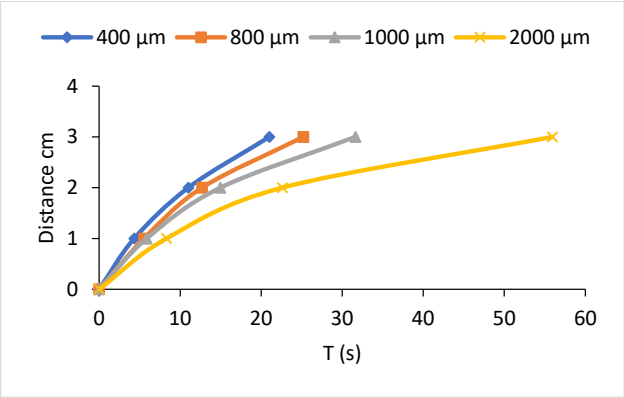
**Figure 5.** Flow velocity comparisons for the fluids across four widths of open microchannels: (**a**) Ethanol-flow speed along various lengths; (**b**) Ethanol-flow speed trend; (**c**) Water-flow speed along various lengths; (**d**) Water-flow speed trend; (**e**) Milk-flow speed along various lengths; (**f**) Milk-flow speed trend; (**g**) Coffee-flow speed along various lengths; (**h**) Coffee-flow speed trend; (**i**) Olive oil-flow speed along various lengths; (**j**) Olive oil-flow speed trend.




(**a**) (**b**)

(**c**) (**d**)

**Figure 6.** *Cont.*

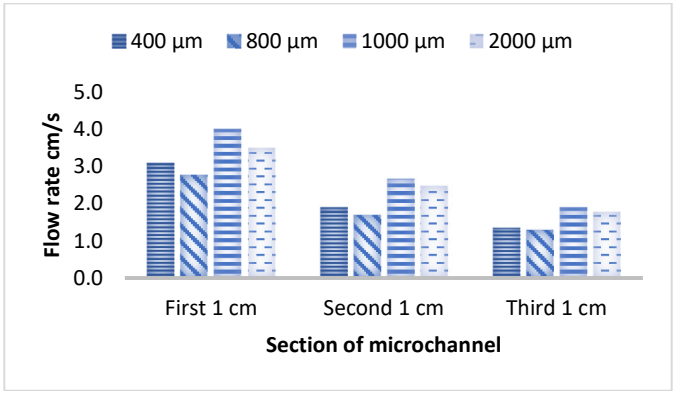



(**e**)

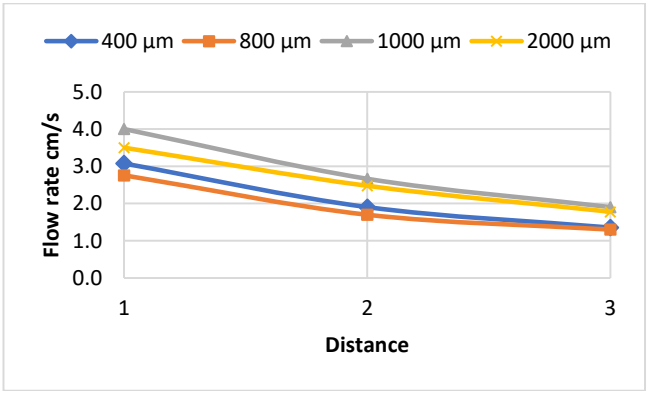
**Figure 6.** The progress of the liquids over time along the length of the open microchannels: (**a**) Ethanol; (**b**) Water; (**c**) Milk; (**d**) Coffee; (**e**) Olive oil.

### *3.2. Flow Velocity of Various Liquids Along Four Sizes of Closed Microchannels*

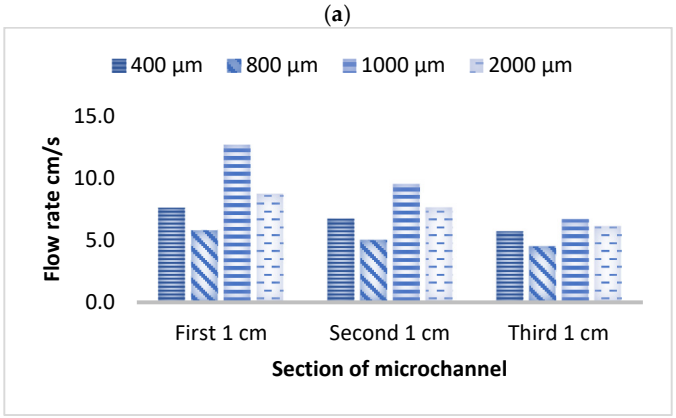
The comparisons of capillary flow velocities for the five selected fluids across four widths of closed microchannels are shown in Figure 7, and the progress of the liquids over time is presented in Figure 8. It is evident that, for all liquids, the flow velocity within the first centimeter of all channels was consistently the highest compared to the second and third centimeters. The flow velocity along the closed microchannel widths showed that the peak velocity is observed along the 1000 µm width, exhibiting the differences in flow behavior between open and closed microchannels.



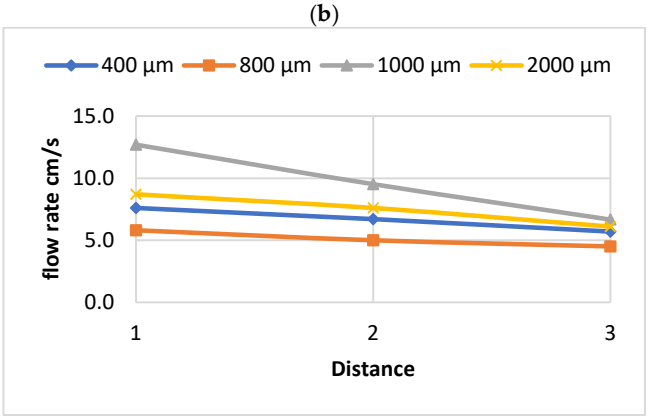

(**a**)




(**b**)

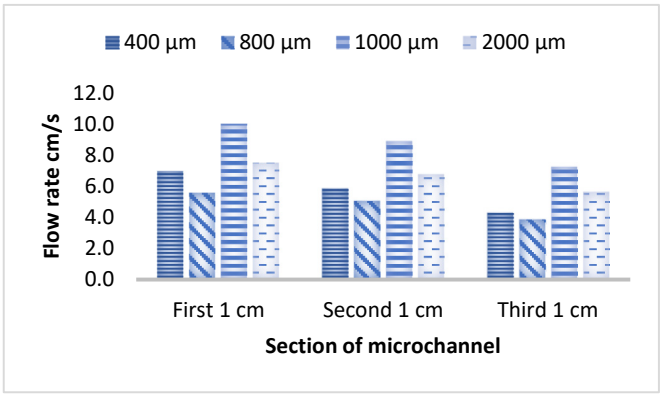



(**c**)

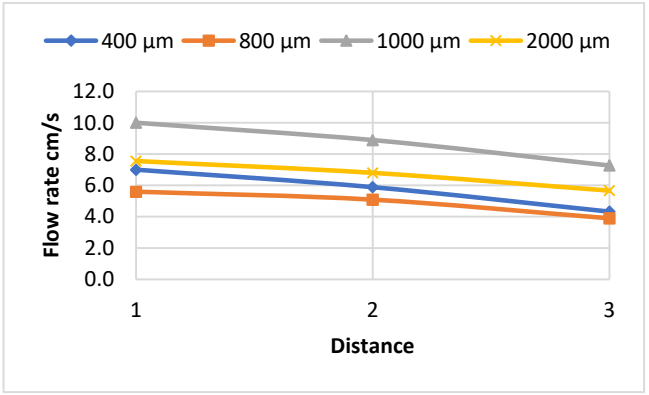



(**d**)

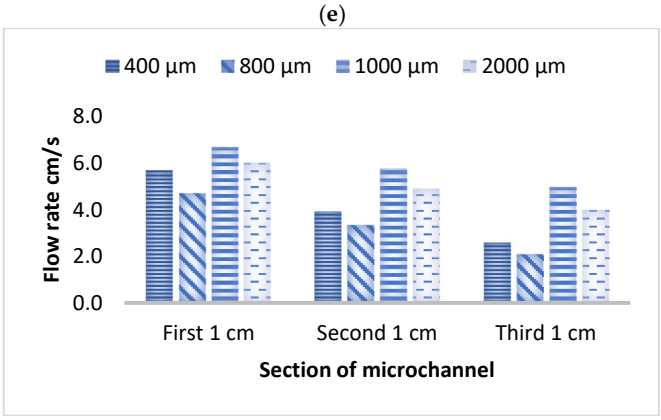
**Figure 7.** *Cont.*



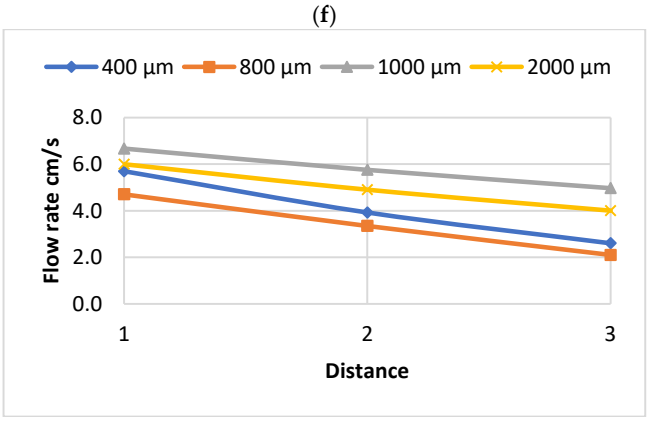

(**e**)



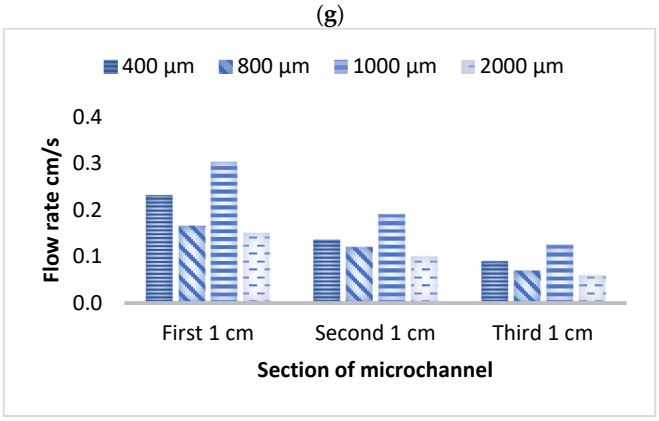

(**f**)



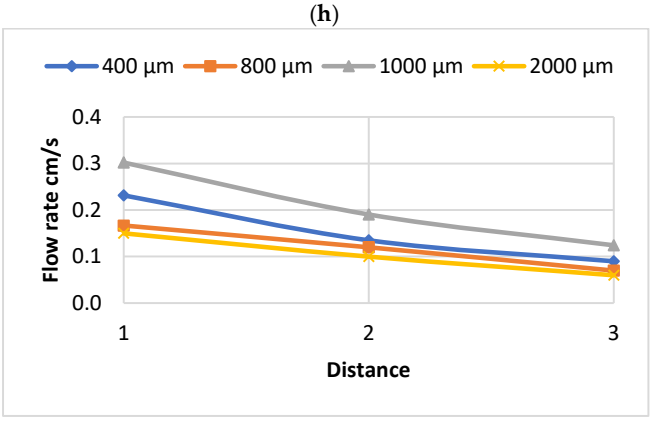

(**g**)




(**h**)




(**i**)




(**j**)

**Figure 7.** Flow velocity comparisons for the fluids across the four widths of the closed microchannel: (**a**) Ethanol-flow speed along various lengths; (**b**) Ethanol-flow speed trend; (**c**) Water-flow speed along various lengths; (**d**) Water-flow speed trend; (**e**) Milk-flow speed along various lengths; (**f**) Milk-flow speed trend; (**g**) Coffee-flow speed along various lengths; (**h**) Coffee-flow speed trend; (**i**) Olive oil-flow speed along various lengths; (**j**) Olive oil-flow speed trend.

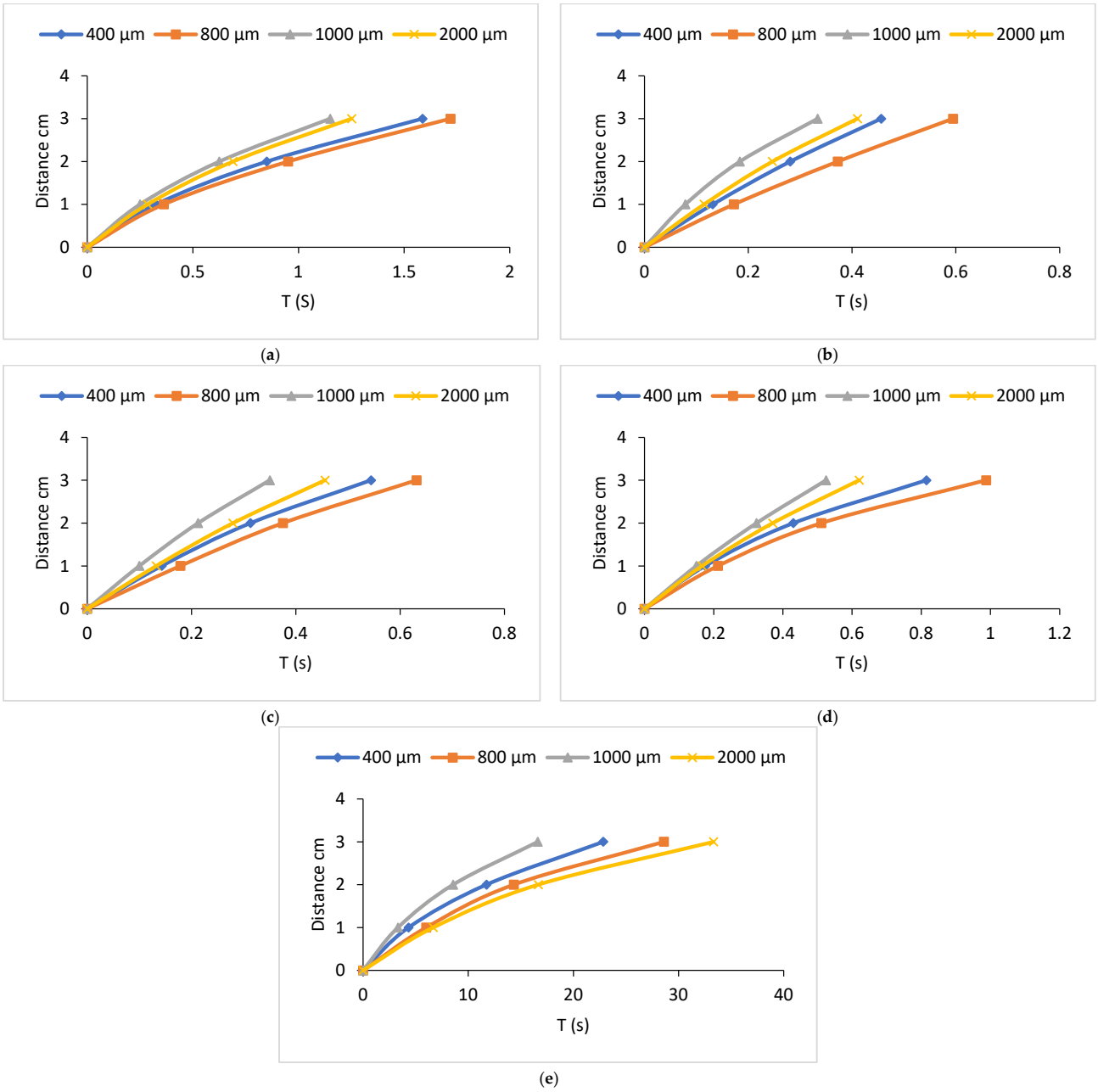



**Figure 8.** The progress of the liquids over time along the length of the closed microchannels: (**a**) Ethanol; (**b**) Water; (**c**) Milk; (**d**) Coffee; (**e**) Olive oil.

The average velocity along the length of the closed microchannels for four widths and five liquids is presented in Figure 9. As can be seen in the figure, among all four widths, the average speeds across the width of 1000 µm were the highest, and across the 800 µm, they were the lowest. Water exhibits the most significant variation in mean fluid velocity among different channel widths, with the lowest value observed across the width of 800 µm and the highest across the 1000 µm widths. This highlights water's distinct sensitivity to changes in microchannel width. In contrast, liquids such as ethanol and olive oil exhibit slight variations, indicating lower dependency on microchannel width. Moreover, it is observed that coffee and milk have almost the same surface tension value, but the viscosity of coffee is three times higher than that of milk, and this caused less flow velocity along the microchannels.

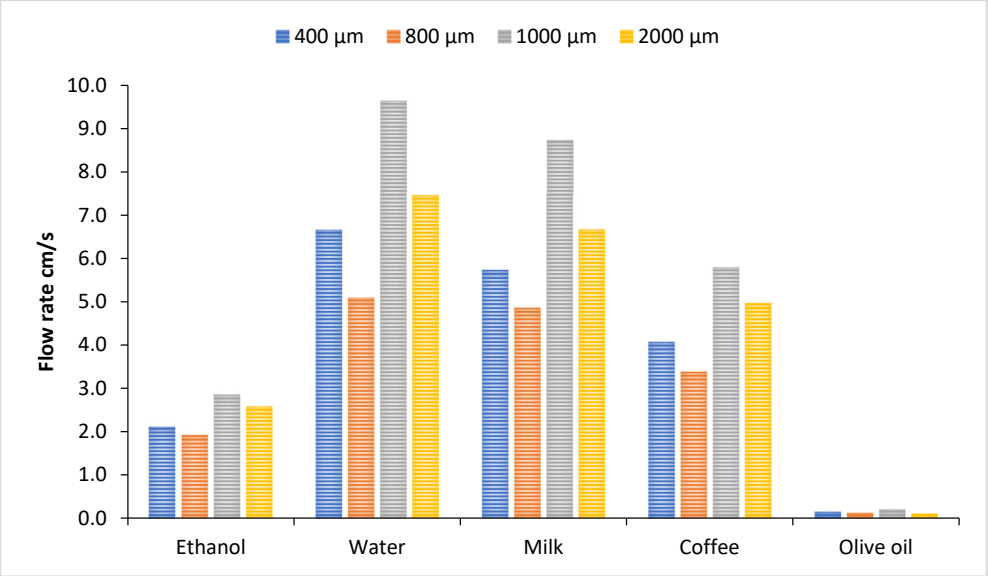



**Figure 9.** The average flow velocity along the length of the closed microchannels.

### *3.3. Theoretical and Experimental Comparisons*

The static contact angles for the used PLA surfaces and PDMS for the five selected liquids are shown in Figure 10. The lowest static contact angles belong to ethanol, and the highest to milk. Figure 10a,b demonstrate the hydrophilicity (both are hydrophilic) of both surfaces. In addition, Figure 10c–j denote that for all selected liquids on PLA and PDMS, the adhesive force is larger than the cohesive force.

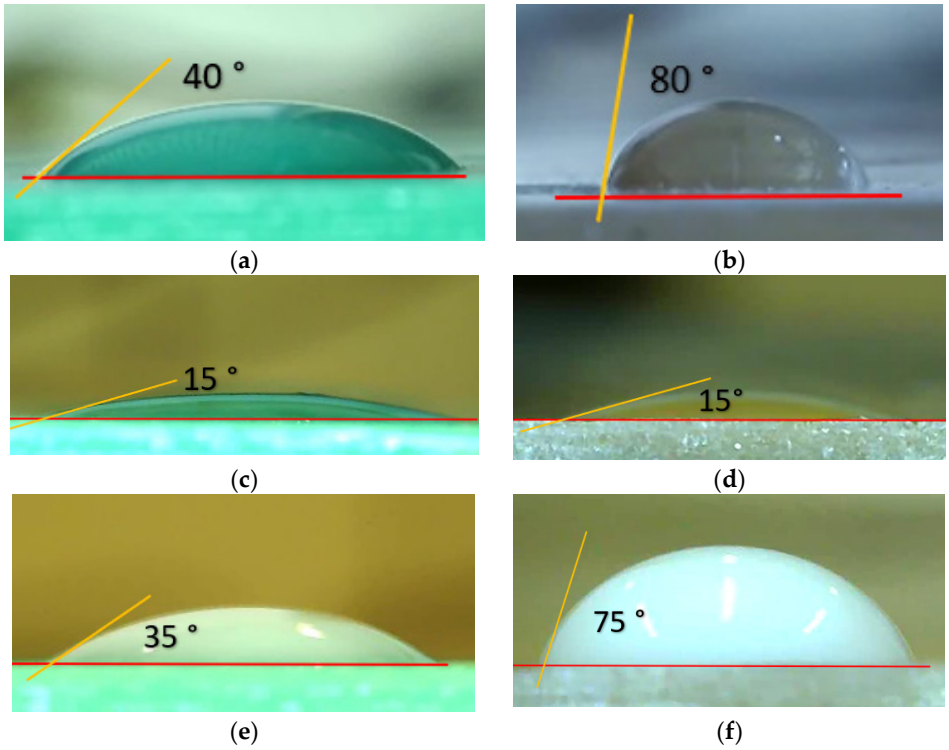



**Figure 10.** *Cont.*

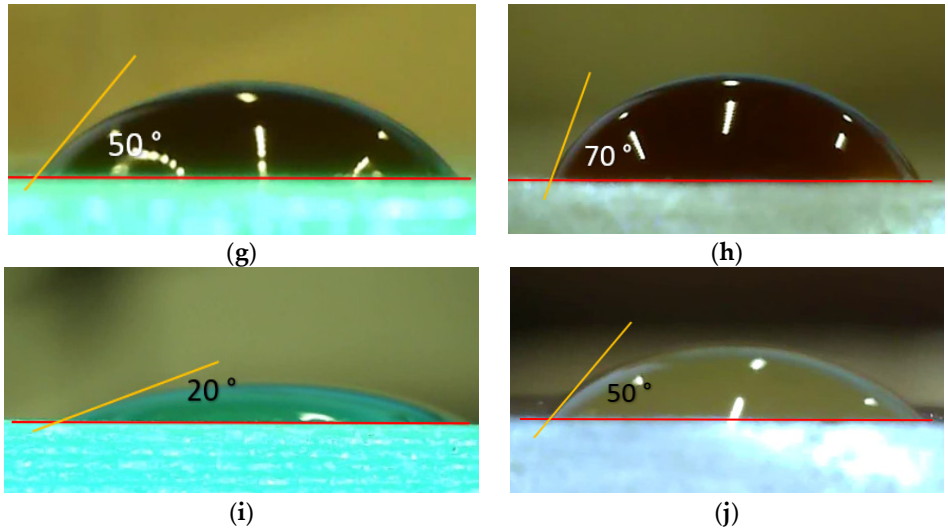



**Figure 10.** The static contact angles for the PLA and PDMS surfaces: (**a**) Water on PLA; (**b**) Water on PDMS; (**c**) Ethanol on PLA; (**d**) Ethanol on PDMS; (**e**) Milk on PLA; (**f**) Milk on PDMS; (**g**) Coffee on PLA; (**h**) Coffee on PDMS; (**i**) Olive oil on PLA; (**j**) Olive oil on PDMS.

The dynamic contact angles within the middle of all channels in open and closed microchannels are presented in Figure 11. In all microchannels, the contact angles were higher in the closed microchannel than in open microchannels, which could be due to the higher contact angles of the PDMS compared to the PLA surface.

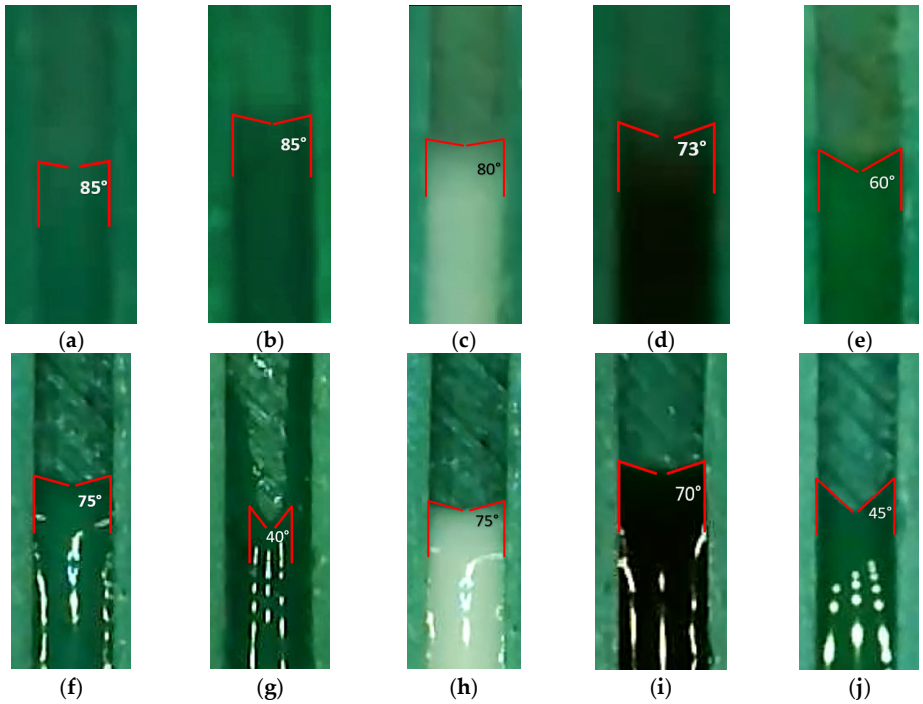



**Figure 11.** Dynamic contact angles in open and closed microchannels: (**a**) Water-closed microchannel; (**b**) Ethanol-closed microchannel; (**c**) Milk-closed microchannel; (**d**) Coffee-closed microchannel; (**e**) Olive oil-closed microchannel; (**f**) Water-open microchannel; (**g**) Ethanol-open microchannel; (**h**) Milk-open microchannel; (**i**) Coffee-open microchannel; (**j**) Olive oil-open microchannel.

Figure 12 presents experimental results for the open microchannel and the closed microchannel with a width of 1000 µm, determining that flow speeds were higher along the closed microchannels. However, except for the water, the speed trends in open and

closed microchannels were similar. The lower values in the open microchannels could be due to the high roughness of the PLA surface compared to the low roughness of the PDMS in the closed microchannels.

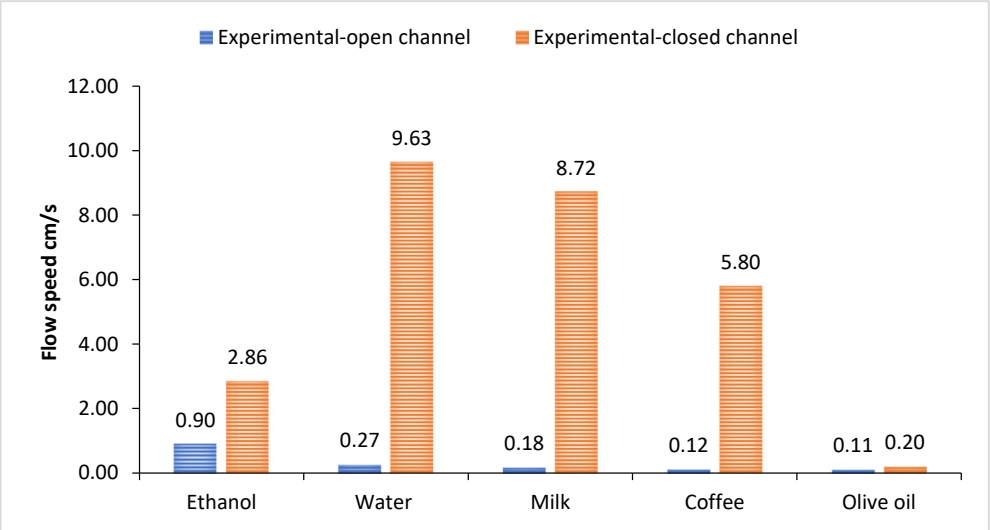



**Figure 12.** The experimental flow speed for the open microchannel and the closed microchannel with a width of 1000 µm.

The theoretical and experimental results for the closed microchannel with a width of 1000 µm were compared, and the comparisons are provided in Table 2. It must be mentioned that the static contact angles for the open microchannels are based on the values in Figure 10 for PLA. For the closed microchannels, as the width and depth are both equal to 1000 µm, the contact angle is calculated based on three surfaces of PLA and one surface of PDMS, which has a higher contact angle. The analysis shows that theoretical values based on static contact angles are overestimated. However, in the closed channel, the theoretical calculations based on dynamic contact angles are similar to the experimental results.

**Table 2.** Comparisons between the theoretical and experimental results for the open microchannel and the closed microchannel with a width of 1000 µm.

| Type of Microchannel | Material | (1) Experimental Velocity (cm/s) | (2) Theoretical Velocity (Dynamic Contact Angle) (cm/s) | (3) Theoretical Velocity (Static Contact Angle) (cm/s) | Relative Error | | |
|---|---|---|---|---|---|---|---|
| | | | | | 2 vs. 1 | 3 vs. 1 | 3 vs. 2 |
| Open | Ethanol | 0.9 | 35.2 | 44.4 | 38.3 | 48.6 | 0.3 |
| | Water | 0.3 | 47.5 | 140.5 | 174.9 | 519.5 | 2.0 |
| | Milk | 0.2 | 15.3 | 48.6 | 82.7 | 263.9 | 2.2 |
| | Coffee | 0.1 | 7.0 | 13.1 | 55.7 | 105.6 | 0.9 |
| | Olive oil | 0.1 | 0.7 | 1.0 | 5.5 | 7.7 | 0.3 |
| Closed | Ethanol | 2.9 | 4.0 | 44.4 | 0.4 | 14.6 | 10.1 |
| | Water | 9.6 | 16.0 | 117.9 | 0.7 | 11.2 | 6.4 |
| | Milk | 8.7 | 10.3 | 41.9 | 0.2 | 3.8 | 3.1 |
| | Coffee | 5.8 | 6.0 | 11.7 | 0.0 | 1.0 | 1.0 |
| | Olive oil | 0.2 | 0.5 | 0.9 | 1.6 | 3.6 | 0.8 |

The results showed overestimations for both theoretical calculations based on static and dynamic angles, while the trend in the dynamic contact angles was similar to the experimental results. The differences between the theoretical and the experimental results could be due to the channel bed's roughness. Moreover, the analysis determined that

while the higher contact angle should result in a higher microfluidic velocity based on the theoretical prediction (as mentioned by Lucas–Washburn), in reality, the irregularities (such as printing orientation) of the microchannel could be a prominent factor. Additionally, in the experimental analysis of the open microchannel with water, at some points, start-stop motion happened, causing lower flow speed than expected capillary flow, which is in agreement with the outcomes of [28] regarding 3D-printed microdevices.

### *3.4. The Factors Affecting the Analysis of 3D Printer-Based Microchannels and Possible Applications*

While the production of microdevices with 3D printers is easy and fast, some critical points need to be considered, including the type, model, print orientation, and filament material of the 3D printers. The zoomed-in images of different parts of the developed boards are shown in Figure 13. As can be seen, there are some irregularities in the different parts of the microchannels and the inlets, which could affect the roughness of the microchannels. The results agree with the study by Lade et al., which showed the impact of different 3D printers and filaments on capillary flow velocity [28,43]. Moreover, print orientation roughness can be observed in the images, which depends on the designer's decision but could affect microfluidic behavior. One also needs to consider plastic roughness, which depends on the 3D printer filament. However, the theoretical equations are also simplified, such as the Lucas–Washburn equation, in which the microdevice material properties or roughness parameters are not considered. Finally, the surface of PLA or other filaments could be hydrophobic or hydrophilic [44–46], impacting the flow pattern, such as the static water contact angle.

To overcome the mentioned issues, the roughness of 3D-printed PLA flat surfaces using FDM can be controlled by adjusting input parameters like layer height, print speed, infill percentage [47], nozzle diameter [48], printing orientation (raster angle) [49], and extrusion temperature [50], as well as by evaluating experimental errors [51]. To account for roughness in theoretical predictions, one can use the effective contact angle on the surface with roughness [52], and by using the effective contact angle in the Lucas–Washburn equation, surface roughness can be considered in theoretical analysis [53].

In realistic applications of 3D-printed microdevices, especially those for medical purposes, one needs to take into consideration that human body fluids, such as blood, are non-Newtonian fluids. The viscosity of blood varies according to force or stress, and during movement, red blood cells (RBCs) may undergo deformation. Nevertheless, dynamic deformation can be disregarded in many cases, and Newtonian models could be applicable [54,55]. In addition, while on the nanoscale, molecular forces need to be considered. On the microscale, the flows can be considered to be a continuum, as the fluids' intermolecular distance, which is about 0.3 nm, can be neglected on the scale of microchannels [56], meaning both classical fluid mechanics (i.e., Navier-Stokes equations) and microfluidic (i.e., Lucas−Washburn equation) theories could be valid [57].

For future studies, the role of elastic turbulence, which is critical in polymer solution flow, as stated by Groisman and Steinberg [58], and the impacts of non-Newtonian flows, as mentioned by Bio et al. [59], on 3D-printed microfluidic devices are recommended for investigation.

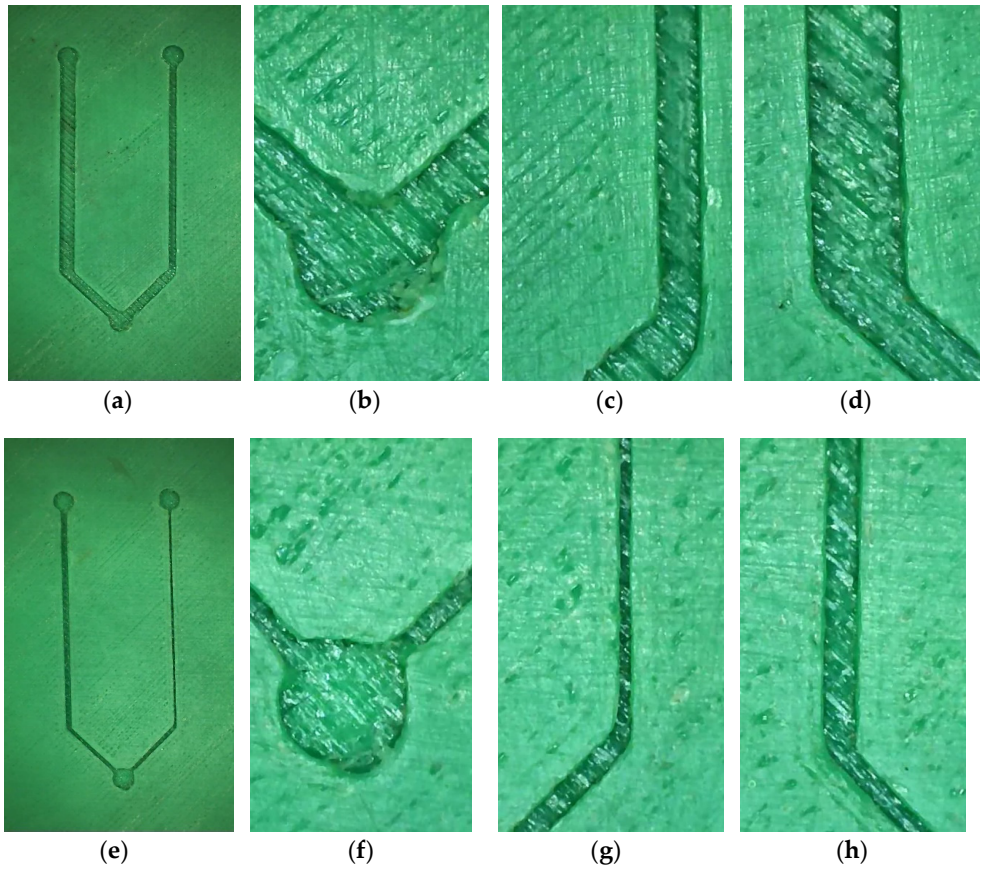



**Figure 13.** The zoomed-in images of different parts of the developed kit: (**a**) The first board with the channels with widths of 1000 μm and 2000 μm; (**b**) The first board inlet; (**c**) A zoomed-in image of the channel with a width of 1000 μm; (**d**) A zoomed-in image of the channel with a width of 2000 μm; (**e**) The second board with the channels with widths of 400 μm and 800 μm; (**f**) The second board inlet; (**g**) A zoomed-in image of the channel with a width of 400 μm; (**h**) The zoomed-in image of the channel with a width of 800 μm.

## 4. Conclusions

This work combined theoretical and experimental results to evaluate the capillary-driven flow of five liquids along open and closed microchannels of four sizes. The investigation of microfluidic velocity demonstrates the peak velocity for open and closed microchannels observed at the beginning, and the velocity decreased with the channel length. Additionally, the maximum average velocity along the open microchannels was observed at a width of 400 μm, while in the closed microchannels, it was observed at a width of 1000 μm, showing differences in flow behavior between open and closed microchannels. The flow velocity values for the selected liquids showed that the highest velocity and lowest viscosity belonged to ethanol and water, and the lowest velocity and highest viscosity belonged to coffee and olive oil, meaning the velocity decreased by increasing the viscosity.

The study of PLA and PDMS surfaces determined that both were hydrophilic (all contact angles were less than 90°), and that the lowest static contact angles belonged to ethanol and the highest to milk. The investigations of dynamic contact angles in open and closed microchannels revealed higher values in the closed microchannel than in open microchannels, which could be due to the higher contact angles of the PDMS compared with the PLA surface. The experimental results revealed higher flow speeds along the closed microchannels than in the open microchannels and nearly the same trend for selected liquids, which could mainly be due to the high roughness of the PLA surface and the low roughness of the PDMS in the closed microchannels. Therefore, it can be concluded that

fluid flow development is not solely dependent on viscosity. Other factors, such as the contact angle of the fluid and surface roughness, must be considered for understanding fluid flow behavior.

Theoretical analysis using the Lucas–Washburn equation with static contact angles demonstrated that the theoretical predictions of flow velocity for all liquids were far lower than the experimental results. These results could be due to simplifications in the theoretical equations, such as the Lucas–Washburn equation, in which the parameters of the microdevice material properties or irregularities caused by 3D printers are not considered. While the theoretical calculations with dynamic contact angles in the closed microchannels were similar to the experimental results, differences in open microchannels were significant but showed the same trends for all liquids. Moreover, the analysis determined that while the higher contact angle should result in a higher microfluidic velocity based on the theoretical prediction, in reality, the irregularities (such as printing orientation) of the microchannel could be the prominent factor. In fact, in 3D-printed microdevices, parameters such as type, model, print orientation roughness, irregularities during print, and the material of the 3D printer, which can be hydrophilic or hydrophobic, are among the other dominant factors.

In conclusion, the results showed the unique behavior of each liquid in different microchannel widths and provided broader information for the better design and fabrication of microdevices using 3D printers.

**Author Contributions:** Conceptualization, B.P.; methodology, B.P., S.N.N. and H.J.N.; software, B.P. and S.N.N.; validation, B.P., S.N.N. and H.J.N.; formal analysis, B.P., D.C. and S.N.N.; investigation, B.P., D.C. and H.J.N.; resources, B.P., D.C. and H.J.N.; data curation, B.P. and S.N.N.; writing—original draft preparation, B.P., S.N.N., D.C. and H.J.N.; writing—review and editing, B.P.; visualization, B.P., S.N.N. and H.J.N.; supervision, P.P.; project administration, P.P.; funding acquisition, P.P. All authors have read and agreed to the published version of the manuscript.

**Funding:** This research received no external funding.

**Data Availability Statement:** The raw data supporting the conclusions of this article will be made available by the authors on request.

**Acknowledgments:** This research was supported by Progetto "Laboratorio Regionale di Ateneo per La Nanomedicina di Precisione Applicata all'Oncologia e alle Malattie Infettive (COVID-19) NLHT—Nanoscience Laboratory for Human Technologies" (Procedura Negoziale ex DGR 459/2020, Asse: Azione 10.5.12, POR Calabria FESR-FSE 14/20) CUP: J29J14001440007.

**Conflicts of Interest:** The authors declare no conflicts of interest.

## Abbreviations

The following abbreviations are used in this manuscript:

| | |
|---|---|
| 3D | Three-dimensional |
| CAD | Computer-Aided Design |
| FDM | Fused deposition modeling |
| FPS | Frames per second |
| HMDS | Hexamethyldisilazane |
| MJM | MultiJet modeling |
| PDMS | Polydimethylsiloxane |
| PLA | Polylactic Acid |
| SLA | Stereolithography |
| SLS | Selective laser sintering |

## References


1. Nielsen, J.B.; Hanson, R.L.; Almughamsi, H.M.; Pang, C.; Fish, T.R.; Woolley, A.T. Microfluidics: Innovations in materials and their fabrication and functionalization. *Anal. Chem.* **2020**, *92*, 150–168. [CrossRef] [PubMed]
2. Watanabe, M. Refreshable microfluidic channels constructed using an inkjet printer. *Sens. Actuators B Chem.* **2007**, *122*, 141–147. [CrossRef]
3. Maria, M.S.; Rakesh, P.E.; Chandra, T.S.; Sen, A.K. Capillary flow-driven microfluidic device with wettability gradient and sedimentation effects for blood plasma separation. *Sci. Rep.* **2017**, *7*, 43457. [CrossRef] [PubMed]
4. Chen, L.; Yang, C.; Xiao, Y.; Yan, X.; Hu, L.; Eggersdorfer, M.; Chen, D.; Weitz, D.A.; Ye, F. Millifluidics, microfluidics, and nanofluidics: Manipulating fluids at varying length scales. *Mater. Today Nano* **2021**, *16*, 100136. [CrossRef]
5. Bhattacharjee, N.; Urrios, A.; Kang, S.; Folch, A. The upcoming 3D-printing revolution in microfluidics. *Lab Chip* **2016**, *16*, 1720–1742. [CrossRef]
6. Koo, D.; So, H. Facile microfabrication of three dimensional-patterned micromixers using additive manufacturing technology. *Sci. Rep.* **2022**, *12*, 6346. [CrossRef]
7. Liu, Y.Z.; Kim, B.J.; Sung, H.J. Two-fluid mixing in a microchannel. *Int. J. Heat Fluid Flow* **2004**, *25*, 986–995. [CrossRef]
8. Schwesinger, N.; Frank, T.; Wurmus, H. A modular microfluid system with an integrated micromixer. *J. Micromech. Microeng.* **1996**, *6*, 99–102. [CrossRef]
9. Di Carlo, D.; Irimia, D.; Tompkins, R.G.; Toner, M. Continuous inertial focusing, ordering, and separation of particles in microchannels. *Proc. Natl. Acad. Sci. USA* **2007**, *104*, 18892–18897. [CrossRef]
10. Harrison, D.J.; Fluri, K.; Seiler, K.; Fan, Z.; Effenhauser, C.S.; Manz, A. Micromachining a miniaturized capillary electrophoresis-based chemical analysis system on a chip. *Science* **1993**, *261*, 895–897. [CrossRef]
11. Palla, A.; Gnecco, I.; Carbone, M.; Garofalo, G.; Lanza, L.G.; Piro, P. Influence of stratigraphy and slope on the drainage capacity of permeable pavements: Laboratory results. *Urban Water J.* **2015**, *12*, 394–403. [CrossRef]
12. Piro, P.; Carbone, M. A modelling approach to assessing variations of total suspended solids (tss) mass fluxes during storm events. *Hydrol. Process.* **2014**, *28*, 2419–2426. [CrossRef]
13. MacDonald, E.; Wicker, R. Multiprocess 3D printing for increasing component functionality. *Science* **2016**, *353*, aaf2093. [CrossRef] [PubMed]
14. He, Y.; Wu, Y.; Fu, J.Z.; Gao, Q.; Qiu, J.J. Developments of 3D Printing Microfluidics and Applications in Chemistry and Biology: A Review. *Electroanalysis* **2016**, *28*, 1658–1678. [CrossRef]
15. Yang, X.; Tang, Q.; Lai, C.; Wu, K.; Shi, X. Applications and Prospects of Microfluidic Chips in Orthopaedic Diseases. *Front. Mater.* **2021**, *7*, 610558. [CrossRef]
16. Fan, X.Y.; Deng, Z.F.; Yan, Y.Y.; Orel, V.E.; Shypko, A.; Orel, V.B.; Ivanova, D.; Pilarsky, C.; Tang, J.; Chen, Z.S.; et al. Application of microfluidic chips in anticancer drug screening. *Bosn. J. Basic Med. Sci.* **2022**, *22*, 302–314. [CrossRef]
17. Illath, K.; Kar, S.; Gupta, P.; Shinde, A.; Wankhar, S.; Tseng, F.G.; Lim, K.T.; Nagai, M.; Santra, T.S. Microfluidic nanomaterials: From synthesis to biomedical applications. *Biomaterials* **2022**, *280*, 121247. [CrossRef]
18. Kolliopoulos, P.; Jochem, K.S.; Johnson, D.; Suszynski, W.J.; Francis, L.F.; Kumar, S. Capillary-flow dynamics in open rectangular microchannels. *J. Fluid Mech.* **2021**, *911*, A32. [CrossRef]
19. Kolliopoulos, P.; Kumar, S. Capillary flow of liquids in open microchannels: Overview and recent advances. *npj Microgravity* **2021**, *7*, 51. [CrossRef]
20. Wenzel, R.N. Resistance of solid surfaces to wetting by water. *Ind. Eng. Chem.* **1936**, *28*, 988–994. [CrossRef]
21. Olanrewaju, A.; Beaugrand, M.; Yafia, M.; Juncker, D. Capillary microfluidics in microchannels: From microfluidic networks to capillaric circuits. *Lab Chip* **2018**, *18*, 2323–2347. [CrossRef] [PubMed]
22. Gorthi, S.R.; Gaikwad, H.S.; Mondal, P.K.; Biswas, G. Surface Tension Driven Filling in a Soft Microchannel: Role of Streaming Potential. *Ind. Eng. Chem. Res.* **2020**, *59*, 3839–3853. [CrossRef]
23. Bernetski, K.A.; An, H.T.; Maki, K.L.; Schertzer, M.J. Predicting actuated contact line pinning forces and the elimination of hysteresis under AC electrowetting. *Microfluid. Nanofluidics* **2022**, *26*, 94. [CrossRef]
24. Keshmiri, K.; Huang, H.; Jemere, A.B.; Nazemifard, N. Investigation of Capillary Filling Dynamics of Multicomponent Fluids in Straight and Periodically Constricted Microchannels. *Langmuir* **2020**, *36*, 6304–6313. [CrossRef]
25. Washburn, E.W. The dynamics of capillary flow. *Phys. Rev.* **1921**, *17*, 273–283. [CrossRef]
26. Yang, D.; Krasowska, M.; Priest, C.; Popescu, M.N.; Ralston, J. Dynamics of capillary-driven flow in open microchannels. *J. Phys. Chem. C* **2011**, *115*, 18761–18769. [CrossRef]
27. Bao, J.; Nagayama, G. Optimization for ultrafast capillary-driven flow in open rectangular microchannels. *Int. J. Heat Mass Transf.* **2023**, *201*, 123629. [CrossRef]
28. Lade, R.K.; Hippchen, E.J.; Macosko, C.W.; Francis, L.F. Dynamics of Capillary-Driven Flow in 3D Printed Open Microchannels. *Langmuir* **2017**, *33*, 2949–2964. [CrossRef]

29. Truesdell, S.L.; Saunders, M.M. A low-cost 3D printed pumping system for generating oscillatory flow in a multicellular lab-on-a-chip device. *Microfluid. Nanofluidics* **2023**, *27*, 42. [CrossRef]
30. ASTM D4212 Standard Test Method for Viscosity by Dip-Type Viscosity Cups. Available online: https://cdn.standards.iteh.ai/samples/115972/31778e8b1a4b497e8b2e5fa689129c34/ASTM-D4212-16-2023-.pdf (accessed on 2 February 2025).
31. Hauner, I.M.; Deblais, A.; Beattie, J.K.; Kellay, H.; Bonn, D. The Dynamic Surface Tension of Water. *J. Phys. Chem. Lett.* **2017**, *8*, 1599–1603. [CrossRef]
32. Tümer, E.H.; Erbil, H.Y.; Akdoğan, N. Wetting of Superhydrophobic Polylactic Acid Micropillared Patterns. *Langmuir* **2022**, *38*, 10052–10064. [CrossRef] [PubMed]
33. Ferner, R.E.; Chambers, J. Alcohol intake: Measure for measure. *BMJ* **2001**, *323*, 1439–1440. [CrossRef] [PubMed]
34. Adamson, A.W.; Klerer, J. Physical Chemistry of Surfaces. *J. Electrochem. Soc.* **1977**, *124*, 192C. [CrossRef]
35. Bertsch, A.J. Surface tension of whole and skim-milk between 18 and 135 C. *J. Dairy Res.* **1983**, *50*, 259–267. [CrossRef]
36. Gmoser, R.; Bordes, R.; Nilsson, G.; Altskär, A.; Stading, M.; Lorén, N.; Berta, M. Effect of dispersed particles on instant coffee foam stability and rheological properties. *Eur. Food Res. Technol.* **2017**, *243*, 115–121. [CrossRef]
37. Illy, E.; Navarini, L. Neglected Food Bubbles: The Espresso Coffee Foam. *Food Biophys.* **2011**, *6*, 335–348. [CrossRef]
38. Calligaris, S.; Mirolo, G.; Da Pieve, S.; Arrighetti, G.; Nicoli, M.C. Effect of Oil Type on Formation, Structure and Thermal Properties of γ-oryzanol and β-sitosterol-Based Organogels. *Food Biophys.* **2014**, *9*, 69–75. [CrossRef]
39. Pirouz, B.; Javadi Nejad, H.; Chirillo, A.S.; Naghib, S.N.; Piro, P. Enhancing the Design of Microdevices: The Role of Computational Fluid Dynamics and Experimental Investigation. *Micromachines* **2025**, *16*, 316. [CrossRef]
40. Lucas, R. Ueber das Zeitgesetz des kapillaren Aufstiegs von Flüssigkeiten. *Kolloid-Z.* **1918**, *23*, 15–22. [CrossRef]
41. Cai, J.; Jin, T.; Kou, J.; Zou, S.; Xiao, J.; Meng, Q. Lucas-Washburn Equation-Based Modeling of Capillary-Driven Flow in Porous Systems. *Langmuir* **2021**, *37*, 1623–1636. [CrossRef]
42. Tokihiro, J.C.; McManamen, A.M.; Phan, D.N.; Thongpang, S.; Blake, T.D.; Theberge, A.B.; Berthier, J. On the Dynamic Contact Angle of Capillary-Driven Microflows in Open Channels. *Langmuir* **2024**, *40*, 7215–7224. [CrossRef] [PubMed]
43. Macdonald, N.P.; Cabot, J.M.; Smejkal, P.; Guijt, R.M.; Paull, B.; Breadmore, M.C. Comparing Microfluidic Performance of Three-Dimensional (3D) Printing Platforms. *Anal. Chem.* **2017**, *89*, 3858–3866. [CrossRef] [PubMed]
44. Ratner, B.D. Surface modification of polymers: Chemical, biological and surface analytical challenges. *Biosens. Bioelectron.* **1995**, *10*, 797–804. [CrossRef] [PubMed]
45. Burg, K.J.L.; Holder, W.D.; Culberson, C.R.; Beiler, R.J.; Greene, K.G.; Loebsack, A.B.; Roland, W.D.; Mooney, D.J.; Halberstadt, C.R. Parameters affecting cellular adhesion to polylactide films. *J. Biomater. Sci. Polym. Ed.* **1999**, *10*, 147–161. [CrossRef]
46. Jiang, Y.; Islam, M.N.; He, R.; Huang, X.; Cao, P.F.; Advincula, R.C.; Dahotre, N.; Dong, P.; Wu, H.F.; Choi, W. Recent Advances in 3D Printed Sensors: Materials, Design, and Manufacturing. *Adv. Mater. Technol.* **2023**, *8*, 2200492. [CrossRef]
47. Jakupi, K.; Dukovski, V.; Hodolli, G. Surface Roughness Modeling of Material Extrusion PLA Flat Surfaces. *Int. J. Polym. Sci.* **2023**, *2023*, 844626. [CrossRef]
48. Buj-Corral, I.; Sánchez-Casas, X.; Luis-Pérez, C.J. Analysis of am parameters on surface roughness obtained in pla parts printed with fff technology. *Polymers* **2021**, *13*, 2384. [CrossRef]
49. Alsoufi, M.S.; Elsayed, A.E. How Surface Roughness Performance of Printed Parts Manufactured by Desktop FDM 3D Printer with PLA+ is Influenced by Measuring Direction. *Am. J. Mech. Eng.* **2017**, *5*, 211–222. [CrossRef]
50. Fountas, N.A.; Kitsakis, K.; Aslani, K.E.; Kechagias, J.D.; Vaxevanidis, N.M. An experimental investigation of surface roughness in 3D-printed PLA items using design of experiments. *Proc. Inst. Mech. Eng. Part J J. Eng. Tribol.* **2022**, *236*, 1979–1984. [CrossRef]
51. Silvestri, L.; Saraceni, M.; Bongioannini Cerlini, P. Quality management system and design of an integrated mesoscale meteorological network in Central Italy. *Meteorol. Appl.* **2022**, *29*, e2060. [CrossRef]
52. Ambrosia, M.S.; Ha, M.Y. A molecular dynamics study of Wenzel state water droplets on anisotropic surfaces. *Comput. Fluids* **2018**, *163*, 1–6.
53. Ouali, F.F.; McHale, G.; Javed, H.; Trabi, C.; Shirtcliffe, N.J.; Newton, M.I. Wetting considerations in capillary rise and imbibition in closed square tubes and open rectangular cross-section channels. *Microfluid. Nanofluidics* **2013**, *15*, 309–326. [CrossRef]
54. Liu, H.; Lan, L.; Abrigo, J.; Ip, H.L.; Soo, Y.; Zheng, D.; Wong, K.S.; Wang, D.; Shi, L.; Leung, T.W.; et al. Comparison of Newtonian and Non-newtonian Fluid Models in Blood Flow Simulation in Patients With Intracranial Arterial Stenosis. *Front. Physiol.* **2021**, *12*, 718540. [CrossRef] [PubMed]
55. Shi, L.; Pan, T.W.; Glowinski, R. Three-dimensional numerical simulation of red blood cell motion in Poiseuille flows. *Int. J. Numer. Methods Fluids* **2014**, *76*, 397–415. [CrossRef]
56. Goetting-Minesky, M.P.; Mullin, B.C. Differential gene expression in an actinorhizal symbiosis: Evidence for a nodule-specific cysteine proteinase. *Proc. Natl. Acad. Sci. USA* **1994**, *91*, 9891–9895. [CrossRef]
57. Tabeling, P. *Introduction to Microfluidics*; Oxford University Press: Oxford, UK, 2023; ISBN 9780192845306.

58. Grolsman, A.; Stelnberg, V. Elastic turbulence in a polymer solution flow. *Nature* **2000**, *405*, 53–55. [CrossRef]
59. Boi, S.; Mazzino, A.; Pralits, J.O. Minimal model for zero-inertia instabilities in shear-dominated non-Newtonian flows. *Phys. Rev. E—Stat. Nonlinear Soft Matter Phys.* **2013**, *88*, 033007. [CrossRef]

**Disclaimer/Publisher's Note:** The statements, opinions and data contained in all publications are solely those of the individual author(s) and contributor(s) and not of MDPI and/or the editor(s). MDPI and/or the editor(s) disclaim responsibility for any injury to people or property resulting from any ideas, methods, instructions or products referred to in the content.